Energy 258 (2022) 124838

Contents lists available at ScienceDirect

Energy

journal homepage: www.elsevier.com/locate/energy

A molecular dynamics study of evaporation of multicomponent stationary and moving fuel droplets in multicomponent ambient gases under supercritical conditions

Yifei Gong [a], Xiao Ma [a,**], Kai Hong Luo [b,*], Hongming Xu [a,c], Shijin Shuai [a]

[a] State Key Laboratory of Automotive Safety and Energy, Tsinghua University, Beijing, 100084, China
[b] Department of Mechanical Engineering, University College London, Torrington Place, London, WC1E 7JE, UK
[c] Department of Mechanical Engineering, University of Birmingham, Birmingham, B15 2TT, UK

ARTICLE INFO

Keywords:
Multicomponent mixing system
Fuel droplet evaporation
Supercritical conditions
Transition criterion
Molecular dynamics

ABSTRACT

The evaporation of a six-component fuel droplet under supercritical conditions is investigated using molecular dynamics (MD) simulations. The focus here is on effects of multicomponent ambient gases and the relative motion between the droplet and the ambient. The ambient pressure ranges from 8 MPa to 36 MPa and the ambient temperature ranges from 750 K to 3600 K. In the lower range of the temperature and pressure, the average displacement increment (ADI) per fuel atom gradually increases with time and the classic evaporation is observed. In the higher range of the temperature and pressure, the ADI profile has a unimodal distribution with time and the diffusive mixing between the droplet and the ambient gases dominates. Based on the ADI profile of fuel atoms, a criterion ($\tau_{0.9P}$) for mode transition from evaporation to diffusion is proposed. Among the ambient gases investigated, the mode transition is the most difficult in the nitrogen ambient but the easiest in combustion exhaust gases. For multicomponent fuel droplets close to or in diffusion mode, with higher relative velocities, the relative difference between evaporation rates for light/heavy fuel components is reduced. This study demonstrates that supercritical conditions alone are insufficient for mode transition of evaporation.

1. Introduction

For most power devices such as liquid rocket engines, to meet more stringent industry requirements, the maximum ambient temperature and pressure in the combustion chamber are getting higher, even exceeding the critical points of injected fuels [1]. The evaporation mode of fuel may transition from classic evaporation to diffusive mixing via transitional mixing under such cases [2]. Many research efforts have been motivated by this phenomenon.

The fuel in combustion chambers is mixed with the ambient gas mainly in the form of droplet evaporation under subcritical conditions, as shown in photographs obtained in typical droplet experiments [3]. However, details about the transition from evaporation to diffusive mixing are hard to obtain by optical measurements [2,4,5]. In the meantime, progresses have been made in CFD simulations of droplet evaporation under supercritical conditions [6–9]. In conventional CFD, it is always assumed that a sharp interface exists between the liquid phase and the gas phase, and the vapor-liquid equilibrium (VLE) is valid. As reported [10], on the other hand, obvious non-VLE behaviors can be observed in single-component fuels under supercritical environments and in binary fuels even in subcritical environments. Moreover, CFD simulations are based on estimated critical points of a chosen system of fuels and ambient gases [11], although these parameters are not accurately determined [12]. These problems are compounded by the fact that theoretical analyses are usually based on the steady-state hypothesis [13] and fail to account for the unsteady nature of evaporation and mode transition [14]. With the rapid development of supercomputers, recent attention has turned to a fundamental method [15], molecular dynamics (MD). Based on Newton's second law, MD computes the motion of individual atoms and/or molecules, which can resolve the vapor-liquid interface with a thickness of a few nanometers, without additional thermodynamic assumptions [16]. As reported [17], drastic changes in the physical properties of a fluid across its thermodynamic critical point make it difficult for CFD to choose the right equation of

* Corresponding author.
** Corresponding author.
E-mail addresses: max@tsinghua.edu.cn (X. Ma), k.luo@ucl.ac.uk (K.H. Luo).

https://doi.org/10.1016/j.energy.2022.124838
Received 18 April 2022; Received in revised form 6 July 2022; Accepted 12 July 2022
Available online 18 July 2022

state (EoS), especially for complex multicomponent fluid systems [12]. MD, on the other hand, makes no assumptions about the physical properties of multicomponent fluids in subcritical and supercritical states [16]. The physical properties are obtained using first-principle methods, and reliable physical property data of supercritical fluids can be obtained [18]. As a result, the fluid property data obtained in MD simulations can provide a reliable benchmark for CFD to employ the correct EoS and mixing rules of components under subcritical and supercritical conditions [19]. Moreover, evaporation is an interfacial behavior that happens in a very thin layer [20]. However, present experiments and conventional CFD are not able to resolve the vapor-liquid interface with a thickness of a few nanometers and thus not suitable to study the mode transition of evaporation. In contrast, MD can exactly resolve the vapor-liquid interface at an atomic level [12]. In this context, MD is a complement to experimental and CFD techniques [19,21]. Because of the large gap in the droplet size investigated in MD simulations and experiments, respectively, efforts have been made to study the size effects in MD simulations [10,17,20,22,23]. In Ref. [17], the droplet size effects on evaporation of single-component fuels have been investigated, no qualitative differences are observed but there are gradual quantitative changes. Similar conclusions have been drawn in Ref. [22]. Due to the complexity of modeling and analysis for multicomponent systems [12,24], most investigations so far have focused on the evaporation of single-component fuels [17,20,25–27]. A few MD studies have focused on surrogate fuels with multi-components (>2) which match better with real fuels [16]. By MD simulations, Zhang et al. [10] concluded that the evaporation of two-component fuels did not meet the assumption of vapor-liquid equilibrium (VLE) under both sub- and supercritical conditions. Gong et al. [12,16] investigated the molecular distributions based on Voronoi tessellations and the molecular interactions between fuel components in multi-component fuels using MD simulations.

Even when multi-component fuels were used, most previous investigations [10,12,16,17,20] replaced actual multi-component ambient gases in the combustion chamber with pure nitrogen (N_2). Such a simplification could be problematic under certain cases. Chakraborty et al. [28] found that when the n-heptane liquid film evaporated in the ambient gas composed of nitrogen and water, the increase in water content promoted the mode transition. Vishnyakov et al. [26,27] considered the VLE of alkanes, and found that results varied significantly among different air components. Wei et al. [29] investigated the injection of sub- and supercritical heptane in a multicomponent ambient composed of water, oxygen and nitrogen; nonetheless, the multicomponent effects on the transition behaviors of fuels were not revealed in detail. He et al. [30] studied the evaporation of fuel droplets and found that the ambient compositions had non-negligible effects on the evaporation rate.

In real engine conditions, there is a large relative velocity between an evaporating droplet and the ambient gas [2,31]. However, in most studies [10,12,16,17,20,25,28], the evaporating film/droplet has no bulk velocity relative to the ambient gas. Direct evidence of the impact of relative velocity on the transition from evaporation to diffusive mixing, especially for multi-component fuels, have been lacking. By theoretical analyses of time scales for several single-component fuels, Poursadegh et al. [31] found that when injected fuels had a high relative velocity, it was inferred the dense-fluid mixing was promoted. Ray et al. [32] investigated the effect of forced convection velocity on the evaporation of a two-component droplet and concluded that the evaporation became faster with increasing relative velocity at all pressures. Recently, Liu et al. [33] studied the effects of forced convection on the preferential vaporization (PV) of multicomponent droplets in detail, however, their research did not cover the supercritical regime.

Building on our previous work on multi-component fuels [12], the present study scrutinizes the evaporation processes of a six-component fuel (a surrogate for diesel) droplet under supercritical conditions using MD simulations. A criterion for mode transition from evaporation to diffusion is introduced, based on the profile of the average displacement increment (ADI) of fuel atoms. According to the ADI criterion, the mode transition map for the six-component fuel droplets in the nitrogen is obtained and is compared with that from experiments [34]. Moreover, effects of ambient multi-component gases on mode transition of evaporation are investigated. Finally, effects of the relative velocity between the droplet and the ambient on the evaporation are revealed.

2. Simulation details

2.1. Interatomic potentials

The MD simulations were carried out using the Large-scale Atomic/Molecular Massively Parallel Simulator (LAMMPS). The United Atom Model (UAM) was chosen to simulate the evaporation of fuels [12]. In this model, an atom group, such as methyl (CH_3), was treated as a specific pseudo-atom. Following our previous work [12], the interactions of fuel molecules are described by the Transferable Potentials for Phase Equilibria United Atom (TraPPE-UA) Model [35]. According to previous reports [35,36], compared with other potential models, the TraPPE-UA model is more suitable for the simulation of long-chain alkane molecules. As the present study focuses on the diesel fuel molecules with long chains, the choice of the TraPPE-UA is justified. The truncated 12-6 Lennard-Jones (LJ) potential is used to describe the non-bonded interaction between pseudo-atoms separated by more than three bonds or belong to two different molecules :

$$U^{LJ}(r_{ij}) = 4\varepsilon_{ij}\left[\left(\frac{\sigma_{ij}}{r_{ij}}\right)^{12} - \left(\frac{\sigma_{ij}}{r_{ij}}\right)^{6}\right] \tag{1}$$

where U^{LJ} denotes the non-bonded LJ interaction potential, ε_{ij} is the energy parameter, σ_{ij} is the size parameter, and r_{ij} is the distance between the two interacting pseudo-atoms. The intermolecular cut-offs were set to 14 Å. The LJ parameters, the bond-stretching, bond bending and bond torsion parameters for alkanes can be found in authors' previous publications [12,16]. The Coulombic pairwise interaction U^{Coul} was added on charged molecules:

$$U^{Coul}(r_{ij}) = \frac{1}{4\pi\varepsilon_0}\frac{q_i q_j}{r_{ij}} \tag{2}$$

where U^{Coul} denotes the Coulombic pairwise interaction, ε_0 is the permittivity of free space. q_i and q_j represent the charges on the two interacting atoms. The coulomb interaction of hydrocarbon fuel molecules and linear diatomic molecules was ignored in the calculation [12]. The force field parameters of molecules of ambient gases are listed in Table 1. The bond lengths of nitrogen molecules and oxygen molecules are fixed as 1.106 Å [17] and 1.21 Å [37] respectively. The bond length of CO_2 ($l_{C\text{-}O}$) is 1.149 Å [38]. The bond length of H_2O ($l_{H\text{-}O}$) is 1 Å [39]. The bond angles of CO_2 and H_2O are 180°and 109.47° respectively [39].

To investigate effects of ambient gases with multi-components on the mode transition of evaporation, this study considers four different ambient gases, marked as "A1", "A2", "A3" and "A4" in turn, whose compositions are shown in Table 2. A1 represents pure N_2, the most commonly used ambient gas during fuel evaporations in MD simulations. According to the simplest air model with multi-components, A2

Table 1
Force field parameters of molecules of ambient gases [16,17,37–39].

atom	ε/k_B[K]	σ [Å]	q [e]
N(in N_2)	36.42	3.32	0
O(in O_2)	49.048	3.013	0
C(in CO_2)	28.129	2.757	+0.6512
O(in CO_2)	80.507	3.033	−0.3256
O(in H_2O)	78.18	3.166	−0.8476
H(in H_2O)	0	0	+0.4238

Table 2
Composition of ambient gases (A1-A4).

Species	A1	A2	A3	A4
N_2	100%	79%	82.2%	87%
O_2	0	21%	12.6%	0
CO_2	0	0	3.5%	8.7%
H_2O	0	0	1.7%	4.3%

consists of only N_2 and O_2 in the standard proportion. Finally, this study referred to the ambient gas composition in the experiment of pre-combustion vessel used by Crua et al. [2], and determined the composition of A3 and A4. The composition was determined by the complete combustion of a mixture composed of acetylene (C_2H_2), O_2 and N_2 in certain proportions:

$$C_2H_2+2.5O_2+2.5XN_2 = 2CO_2+H_2O+2.5XN_2 \quad (3)$$

where X denotes the dilution ratio. Similar to the experimental case by Crua et al. [2], the composition of A4 was determined by the exhaust gas produced by the combustion of C_2H_2 when X = 8 in Equation (3). A3 represents the case where there are some exhaust gases in the ambient gas, which is intended to simulate the exhaust gas recirculation (EGR) that is common in engines. 40% of A3 is exhaust gas from the previous combustion (A4) and the remaining 60% is fresh air (A2).

In earlier studies [12,16], the intermolecular potential model and the surrogate fuel model adopted in the present study were both carefully validated by comparing the VLE data, distillation curves, D^2 curves and evaporation rate constants with experiments. Results have been shown to be in good agreement with experimental data obtained by Ra et al. [40,41]. Moreover, a further comparison was made between the distillation curve of the diesel alternative fuel studied here and that of Fuel CFA (a reference diesel fuel) with thousands of components studied by Charles et al. [42], as shown in Fig. 1. At the whole intermediate stage of distillation, the MD results agree well with the experimental data. At the beginning and near the end of the distillation process, the MD results had acceptable discrepancies with the experimental data (the maximum is around 4%). Overall, the distillation profile of the six-component fuels studied here is in good agreement with that of Fuel CFA [42], suggesting that evaporation data of Fuel CFA [34] can be used for comparisons with simulations results here, which will be discussed later.

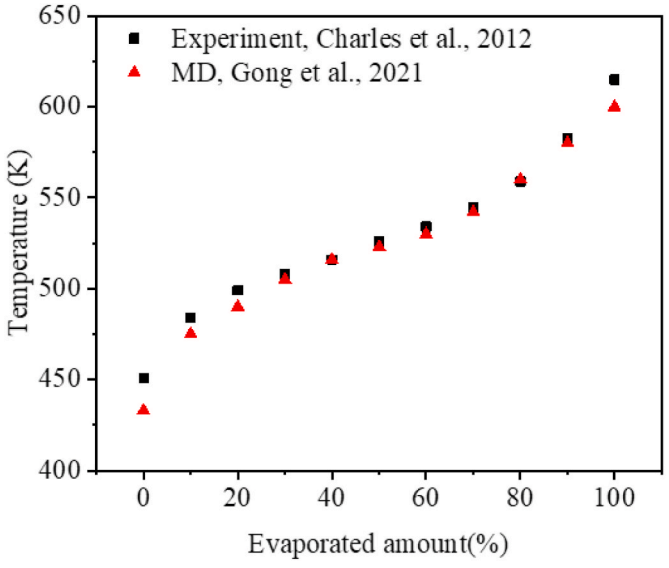

Fig. 1. Comparison of distillation curves of diesel obtained by MD (6-component fuel) and experiments (Fuel CFA). The experimental data are from Ref. [42]. The MD data are from Ref. [12].

2.2. Simulation configurations

The initial configuration of the droplet evaporation system is shown in Fig. 2. In Fig. 2a, a single suspended fuel droplet was located in the center of a cubic box and surrounded by ambient gas molecules. Before the simulation of droplet evaporation, the fuel droplet and the ambient gas were simulated separately using the canonical ensemble (NVT). The boundary of the droplet was defined as the contour surface where the fluid density was equal to the average of the maximum and the minimum densities of the mixing system [12,16,17]. The diameter of the droplet was defined as that of a sphere with the same volume as the droplet [17]. The two were combined together after reaching their own

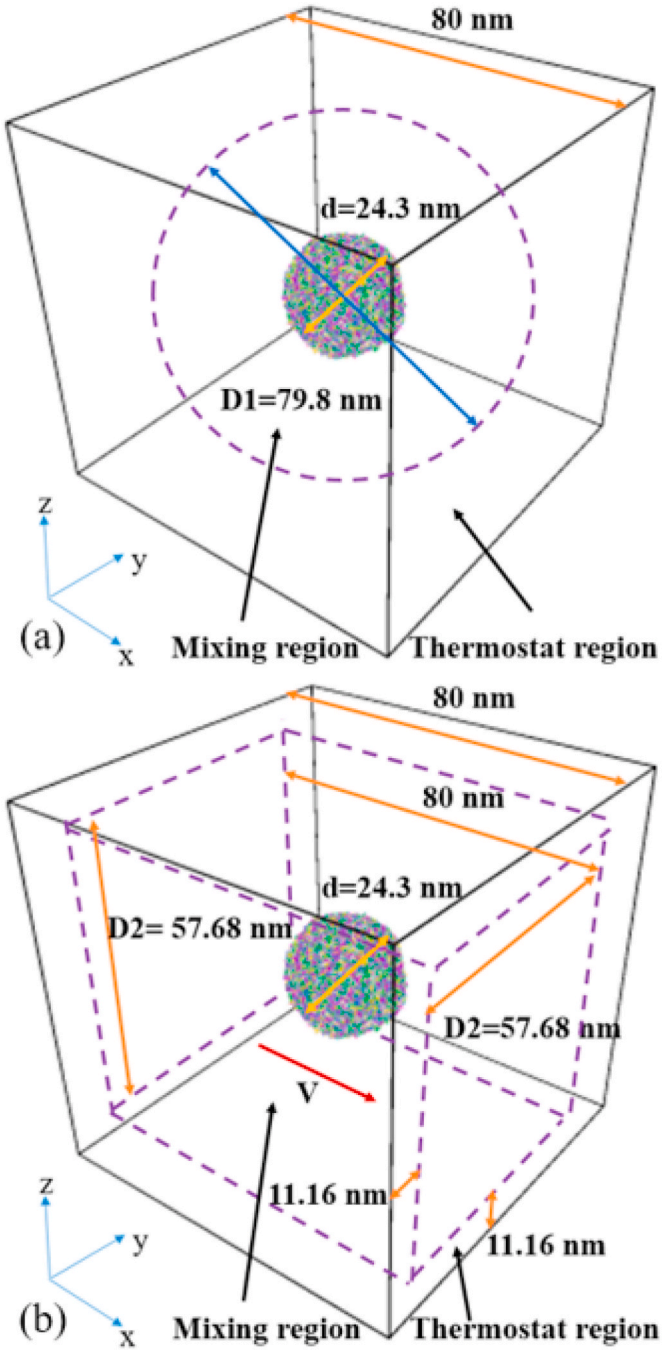

Fig. 2. Initial configurations of the six-component fuel droplet. Ambient gas molecules surround the droplet, which are not shown here: (a) Quiescent case and (b) Non-quiescent case.

thermodynamic equilibrium states. The initial temperature of the fuel was set to 363 K [12]. The side length of the simulation cubic box was 80 nm, and periodic boundary conditions were used in three dimensions. The simulations were performed using the micro-canonical ensemble (NVE). The region outside of the sphere with a radius of 39.9 nm (namely mixing region) was named "thermostat region", in which molecular velocities were rescaled every time step using a speed reset method [16]. A fuel molecule would be deleted when it reached the thermostat region to simulate the evaporation of the droplet taking place in an infinite space [17]. The different initial configurations have been tested before formal simulations. Four replica runs were also had. All other simulation details about the quiescent case (configuration 1) in Fig. 2a can be found in authors' earlier work [12] and are not repeated here. The six-component droplet had an initial diameter of 24.3 nm. The six-component fuel was composed of toluene (13.16 mol %), n-decane (13.81 mol %), n-dodecane (22.30 mol %), n-tetradecane (24.60 mol %), n-hexadecane (14.66 mol %) and n-octadecane (11.47 mol %). More discussions about the size effect in MD simulations and the fuel properties can also be found in Ref. [12]. Considering potential supercritical conditions occurring in rocket engines [20], the target ambient temperature and ambient pressure simulated for the six-component fuel droplet were in the range of 750–3600 K and 8–36 MPa, respectively. Compared with the previous studies [10,12,17,28], the investigated maximum ambient pressure and temperature here were much higher. The time step was 2.0 fs in all cases. The total time steps for a case ranged from 500,000 to 2,500,000 determined by droplet lifetimes [16].

The configuration of the non-quiescent case (configuration 2) was shown in Fig. 2b. The initialization and simulation details of configurations 2 and 1 are the same except for the following two differences. Firstly, in the configuration 2, the center of mass of the droplet moved along the x-direction at a constant speed, and the ambient gas had no macroscopic movement speed. Secondly, the setting of the thermostat region was different. As shown in Fig. 2b, in configuration 2, the mixing region was a rectangular block of 80 nm × 57.68 nm × 57.68 nm. The region outside of the mixing region was exactly the thermostat region, whose volume was kept the same as that in configuration 1. Referring to the experiments by Crua et al. [2], three initial relative velocities of droplets were studied, which were 0 m/s, 30 m/s and 100 m/s, marked as "S", "V1" and "V2" for convenience.

3. Results and discussion

3.1. Effects of ambient pressure and temperature

Ambient temperature and pressure are crucial factors for subcritical to supercritical transition. This study investigated the histories of dimensionless average displacement (AD) and ADI per fuel atom under varied conditions to identify the transition. As mentioned above, the diameter of the droplet was 24.3 nm. The AD and ADI of fuel atoms, as well as the mixing time, have been normalized here. The dimensionless AD and ADI were obtained by dividing their respective values at each moment by the droplet radius (11.75 nm). The dimensionless mixing time, indicated by τ, was obtained by dividing the mixing time by the droplet lifetime. The equations of AD and ADI are as follows:

$$\mathrm{AD}(t^n)=\frac{\sum_{k=1}^{k=m}\sqrt{(X_k(t^n)-0)^2+(Y_k(t^n)-0)^2+(Z_k(t^n)-0)^2}}{m}$$

$$\mathrm{AD}_{\mathrm{R}_0}(t^n)=\frac{\mathrm{AD}(t^n)}{\mathrm{R}_0}$$

$$\mathrm{ADI}(t^n)=\mathrm{AD}(t^n)-\mathrm{AD}(t^{n-1})$$

$$\mathrm{ADI}_{\mathrm{R}_0}(t^n)=\frac{\mathrm{ADI}(t^n)}{\mathrm{R}_0} \quad (4)$$

where t^n indicates the present moment and t^{n-1} indicates the previous moment. The sampling time interval $(t^n - t^{n-1})$ is 0.05 ns. k indicates the identifier of the fuel atoms and m indicates the maximum identifier of the fuel atoms (the total number of fuel atoms) remaining in the simulation domain at time t^n. $\mathrm{AD}(t^n)$ indicates AD at time t^n, and the coordinate of displacement vector of the fuel atom k at time t^n is $(X_k(t^n), Y_k(t^n), Z_k(t^n))$. As stated in Eq. (4), for fuel atom k, the reference position for calculating the displacement magnitude here is its initial position before the evaporation. In other words, the initial coordinate of the displacement vector of fuel atom k is (0, 0, 0). $\mathrm{ADI}(t^n)$ indicates ADI at time t^n. R_0 is the initial droplet radius. $\mathrm{AD}_{\mathrm{R}_0}(t^n)$ indicates the dimensionless AD at time t^n. $\mathrm{ADI}_{\mathrm{R}_0}(t^n)$ indicates the dimensionless ADI at time t^n.

The AD and ADI profiles of fuel atoms have significant differences with time under different ambient conditions, as shown in Fig. 3. At low ambient temperatures and pressures (8 MPa@750 K, case 1), the profile of AD per fuel atom had a concave profile, generally increasing over time, which meant that the mixing became faster and faster. Correspondingly, the ADI of fuel atoms had a gradual increase with time until the end of mixing, as shown in Fig. 3b. At high temperatures and pressures (24 MPa@2100 K, case 2), however, the profile of AD per fuel atom first had a rapid increase over time, but the increase slowed down

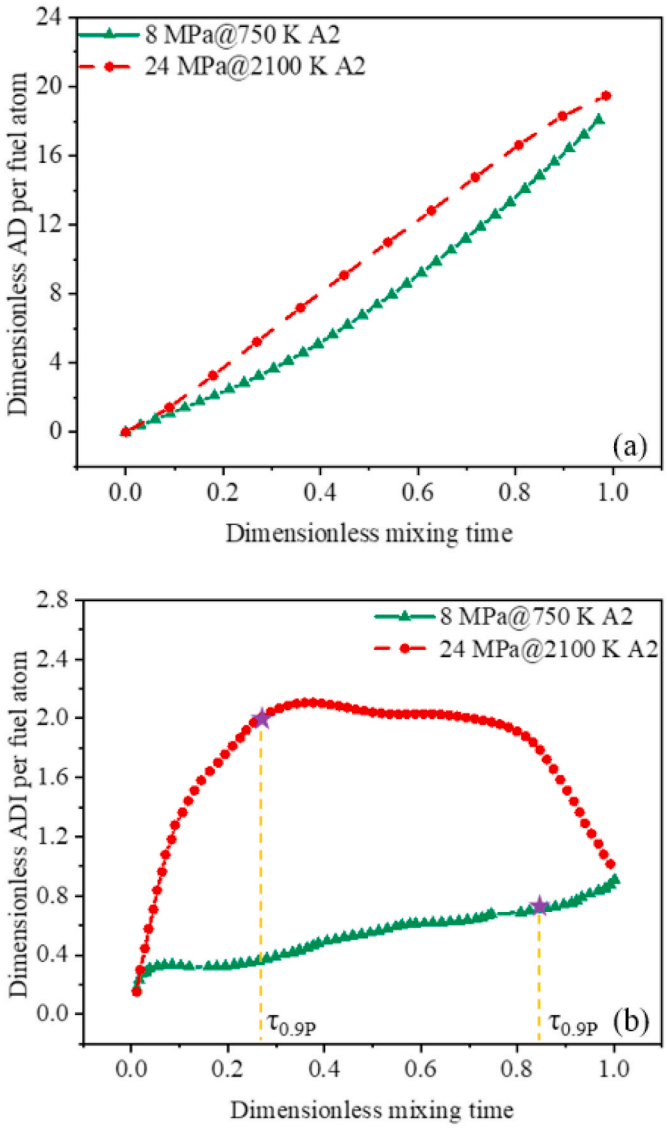

Fig. 3. Dimensionless AD and ADI per fuel atom in different modes.

at later time. Accordingly, the ADI first increased with time, and then gradually decreased after reaching a peak at a certain moment. These differences mean that there are two mechanisms of evaporation. In case 1, the attractions between fuel molecules and the surface tension of the droplet were strong [12,31], and it was hard for ambient gases to dissolve into the droplet via a droplet surface [12]. The order of fuel molecules in the liquid phase was more or less kept. The interaction energy of the liquid fuel was dominant compared with its entropy change. As a result, the ADI of fuel atoms gradually increased with time. The fuel was transformed from liquid phase to gas phase via a phase interface in evaporation mode. In case 2, however, the fuel was transformed from liquid phase to gas phase in evaporation mode initially, when the ADI of the fuel atoms gradually increased with time. However, with rapid transfer of heat and mass under high temperature and pressure, massive ambient gas molecules entered into the fuel droplet and fuel density decreased dramatically [12]. The distances between fuel molecules greatly increased, the attractions between fuel molecules, which was responsible for the molecular order, dramatically declined [12,31]. The original order of fuel molecules in the liquid phase was lost because the entropy change caused by the mixing became dominant. The fuel firstly transitioned from liquid phase to liquid-like phase, and then to gas-like phase, finally to gas phase [22]. When the phase interface completely vanished, the mode transition from evaporation to diffusion was completed. As a consequence, after peaking, the ADI of fuel atoms gradually decreased with time, driven by differences in species concentrations. To easily distinguish the two modes, considering the fluctuations of MD results, this paper defines the dimensionless mixing time corresponding to reaching 90% of the peak value of the ADI profile of fuel atoms for the first time during the mixing as $\tau_{0.9P}$. When $\tau_{0.9P}$ is less than 0.5, it is defined here as the diffusion mode; Otherwise, it is in evaporation mode. This definition is inspired by the experiments by Manin et al. [34], which will be discussed in detail in Fig. 6. Based on this criterion, typical snapshots of molecular distributions of the six-component fuel droplet in different modes are revealed in Figs. 4 and 5. Fig. 4 shows the snapshots under the condition of 8 MPa and 750 K, which is a non-transition case with $\tau_{0.9P}$ of 0.84. During most of the evaporation time of the droplet, the number density of fuel molecules near the interface had a sharp decline and the vapor-liquid interface was easy to recognize. For comparison, Fig. 5 shows the snapshots under the condition of 24 MPa and 2100 K, which is a transition case with $\tau_{0.9P}$ of 0.27. At the same τ (Fig. 5a) as Fig. 4a, the droplet boundary was easily discernible. At $\tau_{0.9P}$ (Fig. 5b), the change of molecular number density of fuels around the droplet was smoother. After that, at the same τ (Fig. 5c) as Fig. 4c, compared with Fig. 4c, the molecular distribution of fuels along the radial direction of the droplet seemed to be quite continuous.

Based on the line of $\tau_{0.9P} = 0.5$, the mode transition map on the P-T diagram for the six-component fuel droplet in nitrogen (A1) is shown in Fig. 6. It is worth noting that a partition criterion with different values of $\tau_{0.9P}$ can be used without affecting the basic conclusions on the mode transition obtained here. As mentioned, MD simulations have inherent randomness. To overcome this, we have 4 replica runs with different initial configurations for each operating condition and the presented results are based on the averages of multiple runs. For each presented case, the repeatability of results is good and the statistical deviations are small. For example, for the case of evaporation under 24 MPa and 2100 K in A2, $\tau_{0.9P} = 0.27 \pm 0.029$ based on 4 runs. Based on the $\tau_{0.9P}$ values, the method of least squares was used to obtain a fitted transition line. As shown in Fig. 6, ten cases around the transition line ($\tau_{0.9P} = 0.5$) were run to get a better fitting, which were indicated by the red square points. The regression model for this transition line with $\tau_{0.9P}$ of 0.5 is as follows (T (unit: K)$\in$[750, 2250], P (unit: MPa)$\in$ [8, 20]):

$$P = 4442.9T^{-0.822} \tag{5}$$

The R2 for this fitting is 0.99. With higher ambient temperatures or pressures, $\tau_{0.9P}$ gradually decreases, and the dominant mode gradually undergoes transition from evaporation to diffusion. Based on the defined critical $\tau_{0.9P}$ (0.5), from Fig. 6, the operating conditions above the transition line could achieve the mode transition from evaporation to diffusion. The results here were compared with experimental data of Fuel CFA from Manin et al. [34], as shown in Fig. 6. Manin et al. [34] studied the mixing regime map of Fuel CFA as it evaporated in the combustion exhaust gas. In the experiments by Manin et al. [34], mixing of fuel droplets is divided into three regimes: classical evaporation, transitional mixing and diffusive mixing. The classical evaporation was characterized by the significant surface tension and existing droplet interface. The transitional mixing was defined for the case where the droplets were observed to deform and oscillate during their evaporation processes, while diffusive mixing referred to a state similar to single-phase mixing caused by the loss of surface tension of the fluid. From this viewpoint, in transitional mixing mode, the transition from evaporation to diffusion is not fully completed, and the droplet surface tension is non-negligible [34]. In addition, from the experimental mixing regime map [34] shown in Fig. 6, compared with the classical evaporation, the area of operating conditions in transitional mixing mode is very small. Based on these, in this paper, the case of transitional mixing and classical evaporation is uniformly defined as the evaporation mode. The brown diamond dots indicated the cases of diffusive mixing in the experiments by Manin et al. [34]. From Fig. 6, the transition line with $\tau_{0.9P}$ of 0.5 obtained here can satisfactorily distinguish the experimental data between transitional mixing and diffusive mixing [34]. Although specifically, there is one experimental diffusive mixing point (T = 1300 K) below the transition line here. That is, the minimum transition pressure at higher ambient temperature (T > 1300 K) from the transition line obtained here on the P-T diagram is slightly higher than that from experiments [34]. This consistency indicates that although there are huge scale differences between experiments and MD simulations, atomistic simulations can reveal fundamental mechanisms that also exist in macroscopic phenomena and thus complement macroscopic experiments. Possible reasons for this difference at high ambient temperature are as follows. Firstly, in terms of experiments, it is quite difficult to accurately identify droplet boundaries by optical devices due to the dense fuel vapor at high temperatures [5], especially for moving

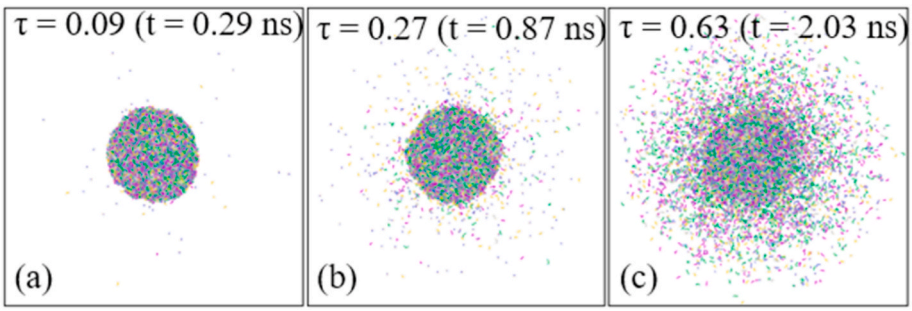

Fig. 4. Snapshots of molecular distributions of the six-component fuel droplet (8 MPa@750 K, A2): (a) $\tau = 0.09$, (b) $\tau = 0.27$ and (c) $\tau = 0.63$. The ambient gas was not shown here.

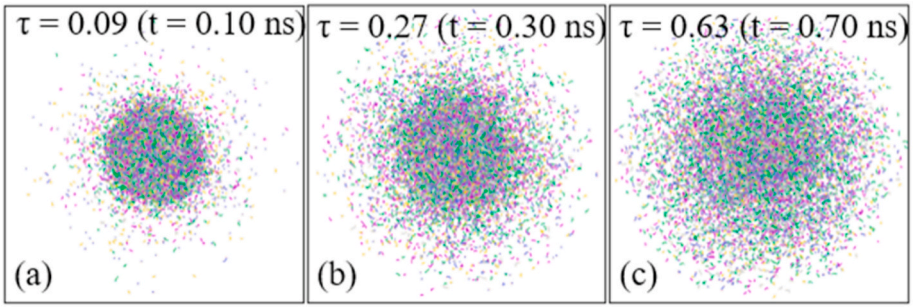

Fig. 5. Snapshots of molecular distributions of the six-component fuel droplet (24 MPa@2100 K, A2): (a) $\tau = 0.09$, (b) $\tau = 0.27$ and (c) $\tau = 0.63$. The ambient gas was not shown here.

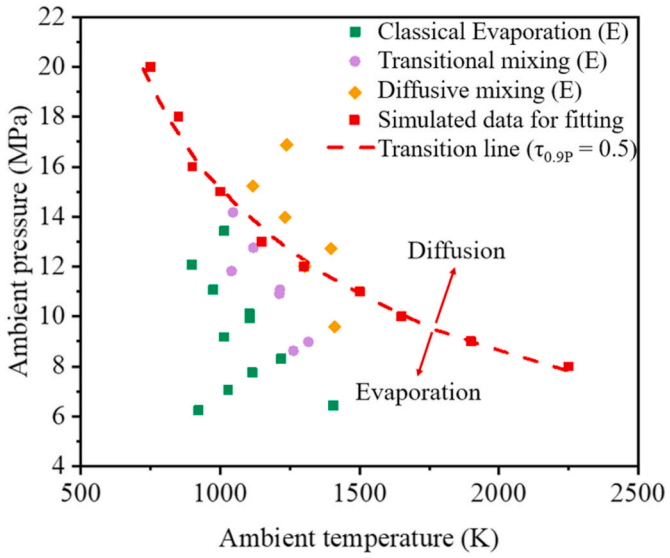

Fig. 6. Mode transition map based on $\tau_{0.9P}$ (A1, S). Here "E" indicates experimental results from Ref. [34].

droplets [2]. Furthermore, as reported [2], optical effects under high pressures, imaging system response and image processing techniques inevitably result in large uncertainties [2]. Thirdly, the simulation results in Fig. 6 are from quiescent droplets, however, droplets with high relative speeds were observed in the optical experiments. As reported [31], the high relative velocities between injected fuels and the ambient gas might promote the transition from classic evaporation to dense fluid mixing, which will also be discussed in the following section. Fourth, the ambient gas in the experiments was combustion exhaust gas [34], not nitrogen used in MD simulations. Based on the following discussion on the multicomponent effects of the ambient gas, the transition in A1 is more difficult than in A4. Size effects might also be responsible for the difference, because the larger droplets, like those in experiments [34], seem to achieve mode transition of evaporation more easily [17]. Besides optical experiments for single- and multicomponent fuels [2,34], similar partition maps were obtained by theoretical analyses [13], CFD simulations [7] and MD simulations [10]. However, those had obvious deficiencies. The theoretical criterion failed when facing the unsteady transition process [13]. The criterion used in traditional CFD simulation was limited to single-component fuels [16]. The criterion based on droplet surface tension at the atomic-level was also problematic because the accurate calculation of surface tension under supercritical conditions in MD simulations was not easy or nearly impossible [43]. The criterion proposed here is based on the ADI of fuel atoms. Independent of the type and number of components in the fuel-ambient gas system, ADI can resolve the mode transition of any fuel-ambient gas system, avoiding deficiencies of previous criteria. For example, the alternative fuel for diesel studied here is derived from Ref. [40]. If the studied fuel is kerosene, the MD research method adopted here is also applicable, because these two fuels are both mixtures containing alkanes, aromatics and other hydrocarbon components. The criterion for the mode transition of evaporation proposed here is also suitable for kerosene. Moreover, in order to further verify its rationality and reliability, we are also studying single-component fuel droplets experimentally investigated by Manin et al. [2]. The existing results show that $\tau_{0.9P}$ of 0.5 is also successful in distinguishing the experimental data between diffusive mixing and transitional mixing of single-component fuels [2].

3.2. *Effects of the composition of ambient gases*

The comparison of $\tau_{0.9P}$ in several types of ambient gases under different ambient conditions is revealed in Fig. 7. With increasing temperature or pressure, $\tau_{0.9P}$ always decreased when the fuel evaporated in any ambient gases investigated. As for the influence of the composition of ambient gases on the mode transition, $\tau_{0.9P}$ gradually decreased with the ambient gas from A1 to A4, meaning that at the same temperature and pressure, the mode transition in nitrogen (A1) was the most difficult. In the combustion exhaust gas (A4), however, the mode transition was the easiest. It is worth noting that, based on Table 2, the relative molecular weight (Mr) of A1, A2, A3 and A4 was 28.01, 28.85, 28.90 and 28.97, respectively. Although the difference is small, it is clear that Mr gradually increases as the ambient gas from A1 to A4. According to Crua et al. [2] and Rezaei et al. [44], at the same ambient temperature and pressure, the higher the Mr of n-alkanes, the greater the possibility

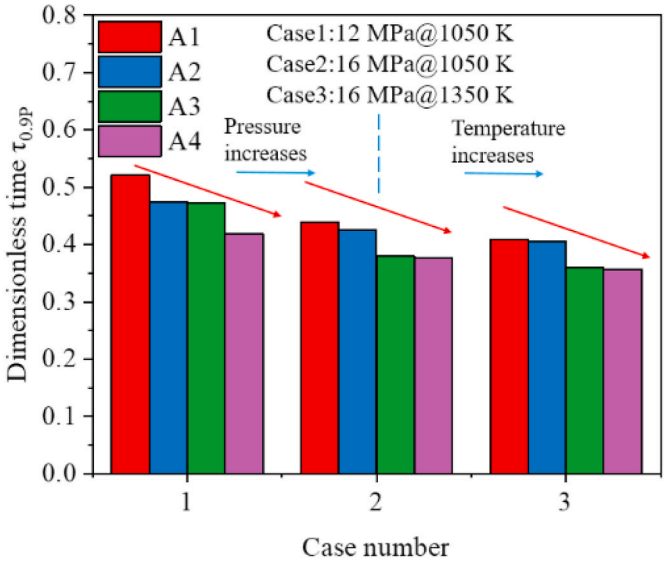

Fig. 7. Comparison of $\tau_{0.9P}$ in different ambient gases.

of transition, even for multicomponent fuels [12]. This study reveals that even for multi-component ambient gases, the larger the Mr of the ambient gas, the smaller the $\tau_{0.9P}$, and the easier the transition, as shown in Fig. 7. This implies that regardless of fuels or ambient gases, their multicomponent effects on the mode transition of evaporation may follow the same physics.

As shown in Fig. 8, histories of AD per fuel atom in ambient gases with different components are investigated. The AD of fuel atoms at the same time gradually increased with the ambient gas from A1 to A4, indicating that the mixing of fuels in nitrogen (A1) was the slowest and the fastest in combustion exhaust gas (A4). Histories of the pair potential energy between fuel components and ambient gas components have also been studied, as shown in Fig. 9. "C_{10}" and "C_{16}" represented the lighter component n-decane and the heavier component n-hexadecane, respectively. As the mixing proceeded, and the pair potential energy increased (pair potential energy was always negative, the discussion refers to its absolute value). Because the fuel molecules were deleted when entering the thermostat region, the pair potential energy decreased gradually after reaching a maximum. Before that, the pair potential energy gradually increased with the ambient gas from A1 to A4, indicating that the pair potential energy between fuel molecules and the nitrogen molecules was the smallest, and that between fuel molecules and exhaust gas molecules was the largest. In addition, the time corresponding to the peak of the pair potential energy profile, which could indicate the mixing speed to a certain extent, gradually decreased with the ambient gas from A1 to A4, consistent with the evolutions revealed in Fig. 8. Note that our analyses are focused on the relative size and time sequence of pair potential profile peaks. The computational domain is large enough relative to the size of the fuel droplets [12,16,17]. The fuel molecules are already in the gas phase when they are removed, and the intermolecular distance is very large, which has little effect on pair potential profile peaks. Snapshots of molecular distributions of the typical components C_{10} and C_{16} in the six-component fuel droplet (12 MPa@1050 K, A1) were revealed in Fig. 10. The time investigated in Fig. 10 was corresponding to the peaks of the pair potential energy profiles of C_{10} and C_{16}, respectively, which was shown in Fig. 9.

3.3. Effects of droplet relative velocity

Previous studies [10,12,28,33] have shown that at lower temperatures and pressures, lighter components evaporate first, followed by heavier ones, which was, namely, the preferential vaporization (PV)

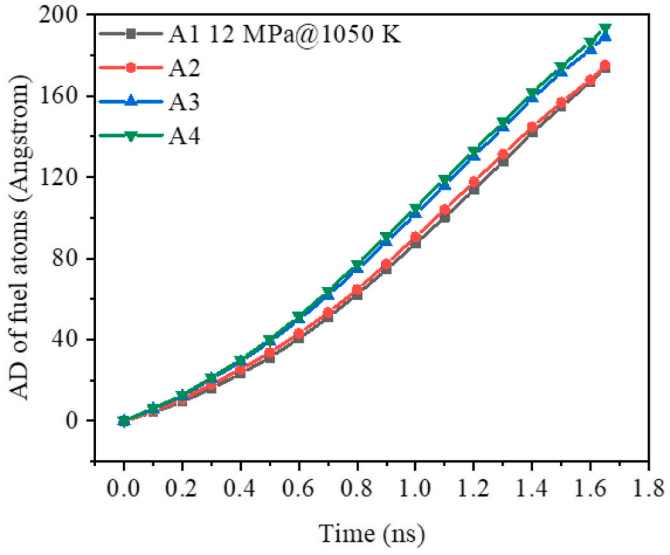

Fig. 8. Histories of AD of fuel atoms.

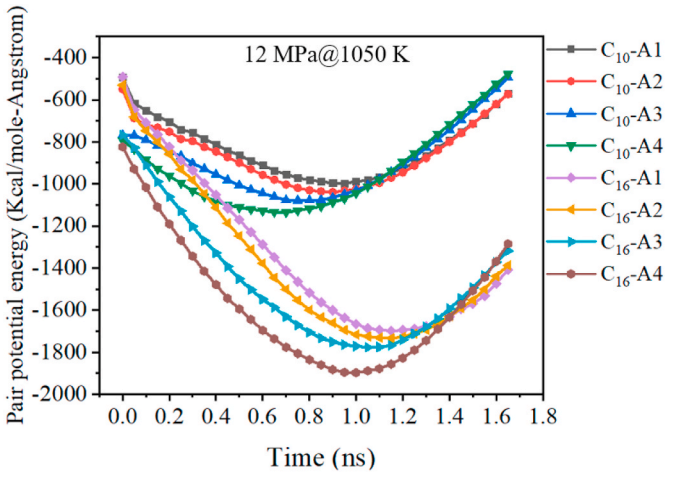

Fig. 9. Histories of pair potential energy between fuel components and ambient gas components.

[33]. Snapshots of molecular distributions of the lightest component C_7 and the heaviest component C_{18} were shown in Fig. 11. The typical PV was observed.

At higher ambient temperatures and pressures, on the other hand, supercritical evaporation occurs and the evaporation rates of light components and heavy ones were simultaneously enhanced [10,28].

To investigate the effect of droplet relative velocity on evaporation, during the period from the start to 90% of C7 had left the droplet, the molecular number of the heaviest component C18 and the lightest component C7 contained in droplets at every moment (the sampling time interval is 0.05 ns) was recorded. To reduce the numerical random errors, the time-averaged number ratio of C18 to C7 was calculated, as shown in Fig. 12. Initially, the molecular number ratio of C18 to C7 was 0.87 (0.87 = 13.16/11.47, as mentioned before). With the increasing droplet relative velocities under the same ambient pressure and temperature, the time-averaged molecular number ratio of C18 to C7 became smaller, which meant that the relative difference in evaporation rates for light/heavy fuel components was reduced, as shown in Fig. 12. In fact, the investigated conditions in Fig. 12 were controlled by the regime of transitional mixing or diffusive mixing (that was, near or in diffusion mode), as shown in Fig. 6. Recently, Liu et al. [33] investigated the PV of RP-3 aviation fuel droplets in the subcritical regime (ambient pressure $P < 2$ MPa) and found that when Re_l (Reynolds number for liquid phase) was less than $Re_{l,c}$ (critical Re_l), with the increasing relative velocities between the droplet and the ambient gas, the PV would be enhanced. The $Re_{l,c}$ for their fuel droplet with a diameter of 0.5 mm was about 0.2 and corresponding critical relative velocity was 0.04 m/s [33]. The droplets investigated here (24.3 nm) are much smaller than 0.5 mm, and the velocities (30 m/s, 100 m/s) are much higher than 0.04 m/s, which means Re_l here was possibly less than $Re_{l,c}$, although the investigated fuels are also different. What requires special attention is that their simulation models were based on the assumption of VLE because their simulations of evaporation were in the subcritical regime [33]. As reported [10], the VLE is invalid in the supercritical regime. This finding will provide an evidence for the more suppressed PV behaviors for non-quiescent multicomponent droplets close to or in diffusion mode compared with quiescent ones.

Histories of the mean square displacement (MSD) of fuel atoms at different droplet relative velocities are shown in Fig. 13. According to the Einstein relationship of MSD [18], the diffusion coefficient of the fuel under the investigated condition (16 MPa@1050 K, A2) was calculated. For case "S, V1 and V2", the molecular diffusion coefficient was 4.5×10^{-7} m^2s^{-1}, 7.0×10^{-7} m^2s^{-1} and 13.6×10^{-7} m^2s^{-1}, respectively. This indicated that the diffusion of fuel molecules was accelerated with increasing droplet relative velocity, consistent with the

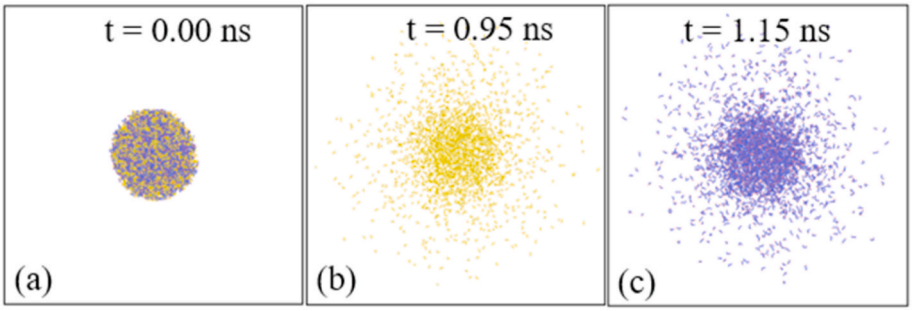

Fig. 10. Snapshots of molecular distributions of the typical components C_{10} and C_{16} in the six-component fuel droplet (12 MPa@1050 K, A1): (a) t = 0.00 ns (C_{10} and C_{16}), (b) t = 0.95 ns (C_{10}) and (c) t = 1.15 ns (C_{16}). The ambient gas was not shown here. Yellow particles represent C_{10} molecules and purple particles represent C_{16} molecules.

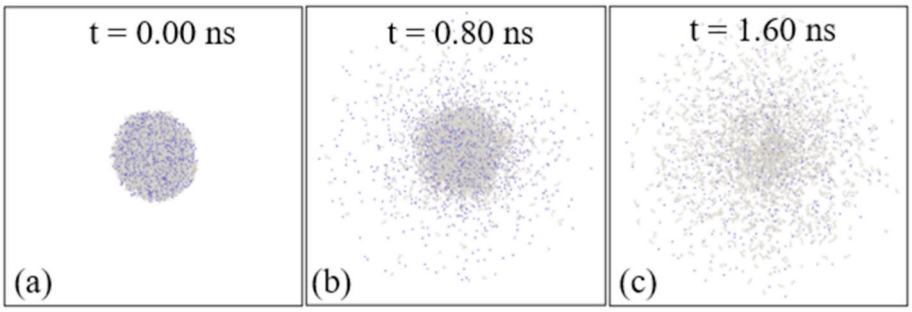

Fig. 11. Snapshots of molecular distributions of the typical components C_7 and C_{18} in the six-component fuel droplet (12 MPa@1050 K, A2, S): (a) t = 0.00 ns ($C_{18}/C_7 = 0.87$, the molecular number ratio), (b) t = 0.80 ns ($C_{18}/C_7 = 1.22$) and (c) t = 1.60 ns ($C_{18}/C_7 = 3.58$). The ambient gas was not shown here. Blue particles represent C_7 molecules and gray particles represent C_{18} molecules.

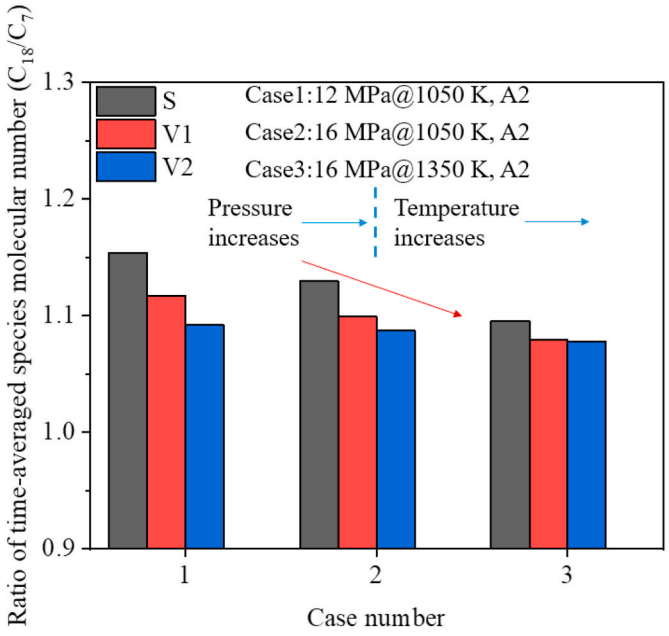

Fig. 12. Ratio of time-averaged species molecular number (C_{18}/C_7) in the fuel droplet when 90% of the C7 has been evaporated at different droplet relative velocities.

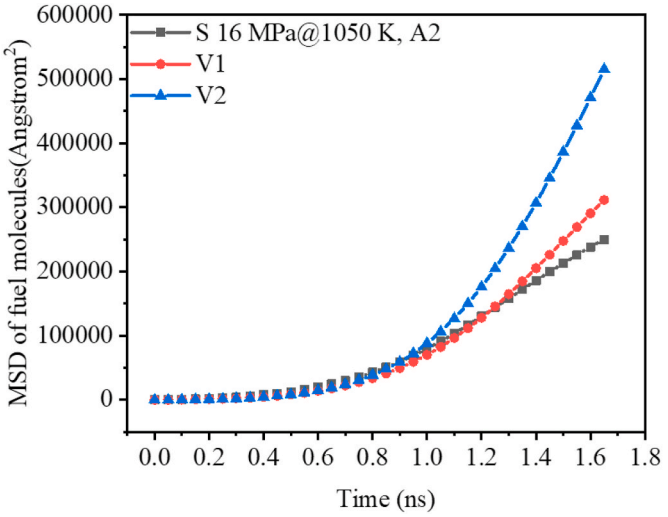

Fig. 13. Comparison of MSD of fuel atoms at different droplet relative velocities.

conclusions by Ray et al. [32] and Liu et al. [33]. In real engine combustion chambers, the typical sizes of droplets are bigger (micron-size). And the turbulent diffusion, which is much stronger than molecular diffusion investigated here, dominates the mass transfer process of the fuel under supercritical conditions [2]. Further work is needed in this area, provided that much supercomputing resources are made available, which is beyond the scope of the present study.

4. Conclusions

In present study, MD was used to investigate the evaporation process of a six-component surrogate fuel droplet in supercritical multi-component ambient gases, focusing on the transition of from classic evaporation to diffusive mixing.

Histories of dimensionless average displacement increment (ADI) of

each fuel atom under varied conditions were investigated. Overall, in the lower range of supercritical temperatures and pressures, the ADI per fuel atom gradually increased with time. In the higher range of supercritical temperatures and pressures, the ADI profile gradually rose to a peak and then declined with time. A criterion ($\tau_{0.9P}$) for transition from evaporation to diffusion is proposed based on the ADI of fuel atoms. It can determine the mode transition of any fuel-ambient gas mixing system at the atomic level, avoiding deficiencies of previous criteria. With increasing temperature or pressure, $\tau_{0.9P}$ gradually decreased, and the evaporation mode of fuels gradually transitioned from classic evaporation to diffusion.

Effects of multi-component ambient gases and the relative velocity between the droplet and the ambient on the mode transition were also investigated. At the same temperature and pressure, in the ambient of nitrogen (A1), air (A2), air with exhaust gas (A3) and exhaust gas (A4), the tendency of mode transition increased in this order, meaning the transition was easier in multicomponent exhaust gases than in pure nitrogen. Consequently, fuel mixed faster in exhaust gas (A4) than nitrogen (A1). For multicomponent fuel droplets near or in diffusion mode, with higher droplet relative velocities, the relative difference between evaporation rates for light/heavy fuel components was reduced. Overall, this study shows that supercritical conditions alone are insufficient for mode transition of evaporation, and a criterion based on the ADI of fuel atoms should be used.

Credit author statement

Yifei Gong: Conceptualization, Methodology, Software, Investigation, Data curation, Visualization, Writing – original draft; Xiao Ma: Conceptualization, Supervision, Funding acquisition, Investigation, Writing – original draft; Kai Hong Luo: Conceptualization, Supervision, Resources, Funding acquisition, Investigation, Writing – original draft; Hongming Xu: Supervision, Project administration; Shijin Shuai: Supervision, Project administration.

Declaration of competing interest

The authors declare that they have no known competing financial interests or personal relationships that could have appeared to influence the work reported in this paper.

Data availability

Data will be made available on request.

Acknowledgements

Support from the Natural Science Foundation of China (Grant No. 51976100) and the UK Engineering and Physical Sciences Research Council under the project “UK Consortium on Mesoscale Engineering Sciences (UKCOMES)” (Grant No. EP/R029598/1) is gratefully acknowledged. This work made use of computational support by CoSeC, the Computational Science Center for Research Communities, through UKCOMES.

References

[1] Riess S, Rezaei J, Weiss L, Peter A, Wensing M. Phase change in fuel sprays at diesel engine ambient conditions: modeling and experimental validation. J Supercrit Fluids 2021;173. https://doi.org/10.1016/j.supflu.2021.105224.
[2] Crua C, Manin J, Pickett LM. On the transcritical mixing of fuels at diesel engine conditions. Fuel 2017;208:535–48. https://doi.org/10.1016/j.fuel.2017.06.091.
[3] Nomura H, Murakoshi T, Suganuma Y, Ujiie Y, Hashimoto N, Nishida H. Microgravity experiments of fuel droplet evaporation in sub- and supercritical environments. Proc Combust Inst 2017;36(2):2425–32. https://doi.org/10.1016/j.proci.2016.08.046.
[4] Manin J, Bardi M, Pickett LM, Dahms RN, Oefelein JC. Microscopic investigation of the atomization and mixing processes of diesel sprays injected into high pressure and temperature environments. Fuel 2014;134:531–43. https://doi.org/10.1016/j.fuel.2014.05.060.
[5] Ghassemi H, Baek SW, Khan QS. Experimental study on binary droplet evaporation at elevated pressures and temperatures. Combust Sci Technol 2006;178(6):1031–53. https://doi.org/10.1080/00102200500296697.
[6] Sazhin SS. Modelling of fuel droplet heating and evaporation: recent results and unsolved problems. Fuel 2017;196:69–101. https://doi.org/10.1016/j.fuel.2017.01.048.
[7] Zhu GS, Aggarwal SK. Transient supercritical droplet evaporation with emphasis on the effects of equation of state. Int J Heat Mass Tran 2000;43:1157–71. https://doi.org/10.1016/S0017-9310(99)00197-0.
[8] Bellan J. Supercritical (and subcritical) fluid behavior and modeling: drops, streams, shear and mixing layers, jets and sprays. Prog Energy Combust Sci 2000;26:329–66. https://doi.org/10.1016/S0360-1285(00)00008-3.
[9] Yang V. Modeling of supercritical vaporization,mixing,and combustion process in liquid-fueled processes in liquid-fueled propulsion systems. Proc Combust Inst 2000;28:925–42. https://doi.org/10.1016/S0082-0784(00)80299-4.
[10] Zhang Y, Jia M, Yi P, Chang Y, He Z, Wang Q. A molecular dynamics study of binary-component n-alkane fuel vaporization characteristics at sub/supercritical nitrogen environments. Proc Combust Inst 2021;38(2):3303–12. https://doi.org/10.1016/j.proci.2020.06.108.
[11] Heidemann RA, Khalil AM. The calculation of critical points. AIChE J 1980;26(5):769–79. https://doi.org/10.1002/aic.690260510.
[12] Gong Y, Luo KH, Ma X, Shuai S, Xu H. Atomic-level insights into transition mechanism of dominant mixing modes of multi-component fuel droplets: from evaporation to diffusion. Fuel 2021;304:121464. https://doi.org/10.1016/j.fuel.2021.121464.
[13] Dahms RN, Oefelein JC. On the transition between two-phase and single-phase interface dynamics in multicomponent fluids at supercritical pressures. Phys Fluids 2013;25(9):92103–27. https://doi.org/10.1063/1.4820346.
[14] Wei Z, Zhou Y, Cao Y, Feng Y, Zhu Q, Zhang Y. Experimental study on the phase inhomogeneity and separability in supercritical state of acetone fuel. Fuel 2022;321. https://doi.org/10.1016/j.fuel.2022.123938.
[15] Tsuda S, Tomi M, Tsuboi N, Ikawa S, Tokumasu T. Extraction of the density fluctuations in diatomic fluids around the critical points using molecular dynamics simulation. J Nanosci Nanotechnol 2015;15(4):3117–20. https://doi.org/10.1166/jnn.2015.9623.
[16] Gong Y, Xiao G, Ma X, Luo KH, Shuai S, Xu H. Phase transitions of multi-component fuel droplets under sub- and supercritical conditions. Fuel 2021;287:119516. https://doi.org/10.1016/j.fuel.2020.119516.
[17] Xiao G, Luo KH, Ma X, Shuai S. A molecular dynamics study of fuel droplet evaporation in sub- and supercritical conditions. Proc Combust Inst 2019;37:3219–27. https://doi.org/10.1016/j.proci.2018.09.020.
[18] Chen C, Jiang X. Transport property prediction and inhomogeneity analysis of supercritical n-Dodecane by molecular dynamics simulation. Fuel 2019;244:48–60. https://doi.org/10.1016/j.fuel.2019.01.181.
[19] Stubbs JM. Molecular simulations of supercritical fluid systems. J Supercrit Fluids 2016;108:104–22. https://doi.org/10.1016/j.supflu.2015.10.027.
[20] Mo G, Qiao L. A molecular dynamics investigation of n-alkanes vaporizing into nitrogen: transition from subcritical to supercritical. Combust Flame 2017;176:60–71. https://doi.org/10.1016/j.combustflame.2016.09.028.
[21] Rahmani F, Weathers T, Hosangadi A, Chiew YC. A non-equilibrium molecular dynamics study of subcritical, supercritical and transcritical mixing of liquid-gas systems. Chem Eng Sci 2020;214:115424–35. https://doi.org/10.1016/j.ces.2019.115424.
[22] Wang Z, Zhou L, Shu G, Wei H. Droplet evaporation and phase transition modes in supercritical environment by molecular dynamic simulation. Phys Fluids 2021;33(6). https://doi.org/10.1063/5.0053328.
[23] Ju D, Huang L, Zhang K, Ye M, Huang Z, Yi G. Comparison of evaporation rate constants of a single fuel droplet entering subcritical and supercritical environments. J Mol Liq 2022;347:118346. https://doi.org/10.1016/j.molliq.2021.118346.
[24] Liu Y, Hong W, Cao B. Machine learning for predicting thermodynamic properties of pure fluids and their mixtures. Energy 2019;188. https://doi.org/10.1016/j.energy.2019.116091.
[25] Lorenzo Consolini SKA, Murad Sohail. A molecular dynamics simulation of droplet evaporation. Int J Heat Mass Tran 2003;46:3179–88. https://doi.org/10.1016/S0017-9310(03)00101-7.
[26] Vishnyakov A, Weathers T, Hosangadi A, Chiew YC. Molecular models for phase equilibria of alkanes with air components and combustion products II. Alkane – oxygen mixtures. Fluid Phase Equil 2020;520. https://doi.org/10.1016/j.fluid.2020.112650. 112650.
[27] Aleksey Vishnyakov TW, Hosangadi Ashvin, Yee C. Chiew. Molecular models for phase equilibria of alkanes with air components and combustion products I. Alkane mixtures with nitrogen, CO_2 and water. Fluid Phase Equil 2020;514. https://doi.org/10.1016/j.fluid.2020.112553. 112553.
[28] Chakraborty S, Qiao L. Molecular investigation of sub-to-supercritical transition of hydrocarbon mixtures: multi-component effect. Int J Heat Mass Tran 2019;145:118629–42. https://doi.org/10.1016/j.ijheatmasstransfer.2019.118629.
[29] Wei W, Liu H, Xie M, Jia M, Yue M. Large eddy simulation and proper orthogonal decomposition analysis of fuel injection under trans/supercritical conditions. Comput Fluids 2019;179:150–62. https://doi.org/10.1016/j.compfluid.2018.10.012.
[30] He R, Yi P, Li T. Evaporation and condensation characteristics of n-heptane and multi-component diesel droplets under typical spray relevant conditions. Int J Heat Mass Tran 2020;163. https://doi.org/10.1016/j.ijheatmasstransfer.2020.120162.

[31] Poursadegh F, Lacey JS, Brear MJ, Gordon RL. On the fuel spray transition to dense fluid mixing at reciprocating engine conditions. Energy Fuels 2017;31(6):6445–54. https://doi.org/10.1021/acs.energyfuels.7b00050.
[32] Ray S, Raghavan V, Gogos G. Two-phase transient simulations of evaporation characteristics of two-component liquid fuel droplets at high pressures. Int J Multiphas Flow 2019;111:294–309. https://doi.org/10.1016/j.ijmultiphaseflow.2018.10.002.
[33] Luo L, Liu YC. Controlling parameters and regimes for preferential vaporization of jet fuel droplet with liquid transport and convection. Fuel 2022;321. https://doi.org/10.1016/j.fuel.2022.123817.
[34] Manin J, Crua C, Pickett LM. In: Transcritical mixing of sprays for multi-component fuel mixtures. ILASS–europe 2017 28th conference on liquid atomization and spray systems; 2017. https://doi.org/10.4995/ILASS2017.2017.5065.
[35] Collin D, Wick MGM, Ilja Siepmann J. Transferable potentials for phase equilibria. 4. United-atom description of linear and branched alkenes and alkylbenzenes. J Phys Chem B 2000;104:8008–16. https://doi.org/10.1021/jp001044x.
[36] Marcus G, Martin JIS. Transferable potentials for phase equilibria. 1. United-atom description of n-alkanes. J Phys Chem B 1998;102. https://doi.org/10.1021/jp972543+.
[37] Hansen N, Agbor FAB, Keil FJ. New force fields for nitrous oxide and oxygen and their application to phase equilibria simulations. Fluid Phase Equil 2007;259(2):180–8. https://doi.org/10.1016/j.fluid.2007.07.014.
[38] Harris JG, Yung KH. Carbon dioxide's liquid-vapor coexistence curve and critical properties as predicted by a simple molecular model. J Phys Chem 1995;99:12021–4. https://pubs.acs.org/doi/pdf/10.1021/j100031a034.
[39] Taylor RS, Dang LX, Garrett BC. Molecular dynamics simulations of the liquid/vapor interface of SPC/E water. J Phys Chem 1996;100:11720–5. https://doi.org/10.1021/jp960615b.
[40] Ra Y, Reitz RD. A vaporization model for discrete multi-component fuel sprays. Int J Multiphas Flow 2009;35(2):101–17. https://doi.org/10.1016/j.ijmultiphaseflow.2008.10.006.
[41] Butts RT, Foster D, Krieger R, Andrie M, Ra Y. Investigation of the effects of cetane number, volatility, and total aromatic content on HighlyDilute low temperature diesel combustion. SAE Int 2010. https://doi.org/10.4271/2010-01-0337.
[42] Mueller CJ, Cannella WJ, Bruno TJ, Bunting B, Dettman HD, Franz JA, et al. Methodology for formulating diesel surrogate fuels with accurate compositional, ignition-quality, and volatility characteristics. Energy Fuels 2012;26(6):3284–303. https://doi.org/10.1021/ef300303e.
[43] Ghoufi A, Malfreyt P, Tildesley DJ. Computer modelling of the surface tension of the gas–liquid and liquid–liquid interface. Chem Soc Rev 2016;45(5):1387–409. https://doi.org/10.1039/c5cs00736d.
[44] Rezaei J, Riess S, Wensing M. Phase change in fuel sprays at diesel engine ambient conditions: impact of fuel physical properties. J Supercrit Fluids 2020;170. https://doi.org/10.1016/j.supflu.2021.105224.